Available online at www.sciencedirect.com
ScienceDirect
International Journal of Heat and Fluid Flow 29 (2008) 107–118
International Journal of HEAT AND FLUID FLOW
www.elsevier.com/locate/ijhff

Effect of radiative heat transfer on the three-dimensional Boyancy flow in cubic enclosure heated from the side

Mohamed Naceur Borjini [a], Habib Ben Aissia [b], Kamel Halouani [c], Belkacem Zeghmati [d,*]

[a] Département de Physique, Faculté des Sciences, 5019 Monastir, Tunisie
[b] Ecole Nationale d'Ingénieurs, 5012 Monastir, Tunisie
[c] METS–ENIS–IPEIS, Route Menzel Chaker, B.P. 805, 3000 Sfax, Tunisie
[d] MEPS-GME, Université de Perpignan Via Domitia, 52 Avenue Paul Alduy, 68860 Perpignan Cedex, France

Received 3 March 2006; received in revised form 22 January 2007; accepted 17 July 2007
Available online 23 October 2007

Abstract

This article presents a numerical study of the effect of the radiative heat transfer on the three-dimensional convection in a cubic differentially heated cavity for different optical parameters of the medium, $Pr = 13.6$ and $Ra = 10^5$. The natural convection equations, using the Boussinesq approximation for the treatment of buoyancy term in the momentum equation, are expressed using the vorticity-stream function formulation. These equations and the radiative transfer equation are discretized, respectively, with the control volume finite difference method and the FTn finite volume method. The successive relaxation-iterating scheme is used to solve the resultant algebraic system equations. Results show that the structure of the main flow is considerably altered by of the conduction–radiation parameter. The inner spiraling flows are found very sensible in location and direction to the radiative heat transfer. However, the peripheral spiraling motion is qualitatively insensitive to these parameters. It is also found that radiation favorites the merging of the vortices near the front and back walls.

Keywords: 3D natural convection; Radiation; Spiral flow

1. Introduction

Natural convection in differentially heated rectangular enclosure has received considerable attention in the recent heat transfer studies (Mallinson and de Vahl Davis, 1977; Lee et al., 1988; Fusegi et al., 1991a,b, 1992; Salat et al., 2004, etc.). For air filled cavity the flow is stable for Rayleigh number $Ra < \approx 10^6$ and manifests one or two vortices pattern at the XY-mid-plane (Fig. 1). For higher values of Ra, oscillations appear and the flow becomes unstable. In recent times, Tric et al. (2000) benchmark this problem using a pseudo-spectral Chebyshev algorithm. A latest analysis of benchmark numerical studies for 3D natural convection in an air filled cubic cavity is effectuated by Pepper and Hollands (2002). More recently, Wakashima and Saitoh (2004) used the high-order time–space method to benchmark this problem. Janssen et al. (1993) studied the transition to time periodicity in such problem and mentioned that the corresponding period is almost the same as for 2D square cavity but the distribution of the amplitude of the oscillations is remarkably three-dimensional. Mallinson and de Vahl Davis (1977) and Fusegi et al. (1991a) analyzed the three-dimensional structure of the flow. Similar works exist for liquid–metals (Viskanta et al., 1986; Henry and Buffat, 1998; Juel et al., 2001; Piazza and Ciofalo, 2002, etc.) and high Prandtl number fluids (Hiller et al., 1989, 1990).

As mentioned above, the main flow observed at the mid plane or by 2D modeling presents one or two vortices

* Corresponding author.
E-mail addresses: naceur.borjini@fsm.rnu.tn (M.N. Borjini), Habib.benaissia@enim.rnu.tn (H. Ben Aissia), zeghmati@univ-oerp.fr (B. Zeghmati).

0142-727X/$ - see front matter © 2007 Elsevier Inc. All rights reserved.
doi:10.1016/j.ijheatfluidflow.2007.07.012

Nomenclature

g	acceleration of gravity
I	dimensionless radiant intensity, $I = I'/(n^2\sigma (T'_c)^4/\pi)$
I^0	dimensionless black body intensity, $I^0 = I^{0\prime}/(n^2\sigma(T'_c)^4/\pi)$
L	total number of discrete solid angles
L_+	total number of discrete solid angles oriented to a given boundary
N	dimensionless quantity, $N_i^l = \frac{1}{\Delta\Omega^l}\int_{\Delta\Omega^l} \mathbf{\Omega}.n_i \,\mathrm{d}\Omega$
n	refractive index
n	unit vector normal to the control volume surface
Pr	Prandtl number, $Pr = \nu/\alpha$
q_c	dimensionless local conductive heat flux on isothermal walls
q_r	dimensionless local radiative heat flux on isothermal walls
Ra	Rayleigh number, $Ra = \beta_T g(T'_h - T'_c)W^3/(\nu\alpha)$
Rc	radiation conduction parameter, $\mathrm{Rc} = n^2 W T_c^3 \sigma/\lambda$
s	distance in the direction $\mathbf{\Omega}$ of the intensity
S	Stratification factor $\left(\frac{\partial T}{\partial y}\right)$
T	dimensionless temperature, $T = (T' - T'_c)/(T'_h - T'_c)$
t	dimensionless time, $t = \alpha t'/W^2$
T'_h	hot wall temperature
T'_c	cold wall temperature
$\vec{V}$	dimensionless velocity $\vec{V} = \vec{V}'W/\alpha$
W	enclosure width
x, y, z	dimensionless Cartesian coordinates, $x = x'/W$, $y = y'/W$, $z = z'/W$

Greek symbols

α	thermal diffusivity
β_T	coefficient of thermal expansion
β_r	extinction coefficient, $\beta_r = \sigma_r + \kappa$
ΔA	area of a control volume face
Δv	control volume
$\Delta\Omega$	control solid angle
ε	emissivity
Φ	temperature ratio, $\Phi = T'_h/T'_c - 1$
κ	absorption coefficient
λ	thermal conductivity
ν	kinematic viscosity
σ	Stefan–Boltzmann constant
σ_r	scattering coefficient
τ	optical width, $\tau = \beta_r W$
$\vec{\omega}$	dimensionless vorticity vector, $\vec{\omega} = \vec{\omega}'W^2/\alpha$
ω_0	scattering albedo, $\omega_0 = \sigma_r/\beta_r$
$\mathbf{\Omega}$	unit vector in the direction of the intensity
$\vec{\phi}$	dimensionless vector potential, $\vec{\phi} = \vec{\phi}'/\alpha$

Subscript

e, w, n, s, t, b	faces of control volume centered in P
E, W, N, S, T, B	nodes around the nodal point P
P	nodal points

Superscript

$'$	real variables
l, l'	discrete angular directions
1	x-component
2	y-component
3	z-component

transporting the fluid back and forth between the isothermal walls. The three-dimensional flow structure consists of one or two inner spiraling motions sustaining the transverse flow between the front or back walls and the center of the box and a large spiraling flow near the lateral walls. This is partially proved in the revealing experimental work of Hiller et al. (1989) which brings to the fore the spiraling character of the 3D flow of 6000-Prandtl number liquid. In fact, in the neighborhood of the vortices centers, the flow spirals from the back and front walls toward the XY-mid-plane and conversely in the outer regions. About midway between this plane and the front or back walls, one of these vortices disappears and the second vortex appears to be twisted with its ends around the first one. These inward spiral circulation in the center and outward circulation near the side walls are already predicted by the numerical work of Mallinson and de Vahl Davis (1977). However, some differences between the two results exist and Hiller et al. (1989) explain this by the Boussinesq approximation and the imperfect adiabatic condition on the non-isothermal walls. The last hypothesis is envisaged by several works (Le Peutrec and Lauriat, 1990; Fusegi et al., 1991b; Fusegi and Hyun, 1994; Kowalewski, 1998; Leonardi et al., 1999). In particular, Kowalewski (1998) and Leonardi et al. (1999) highlight the important effect of the thermal boundary conditions (TBC) at these walls on this spiraling flow. In fact, the shape, the location of the merging region, direction and pitch of the inner spirals are extremely sensitive to the TBC at the non-isothermal walls. They suggest the implementation of measured temperature fields as thermal boundary conditions. The authors also checked out the effect of initial conditions and variables properties on the z component of velocity responsible of the transverse flow. For water-glycerin solution, the effect of variable fluid properties appeared to be secondary compared with effects of the TBC. Likewise, in the Rayleigh–Benard convection, the effect of the TBC on the 3D behavior is primordial (Kessler, 1987).

This cross flow is also identified in liquid–metals and in the limiting case of zero Prandtl number. Viskanta et al. (1986) mentioned that, for low values of Prandtl number, the 3D effects are extended down to the mid-plane of the

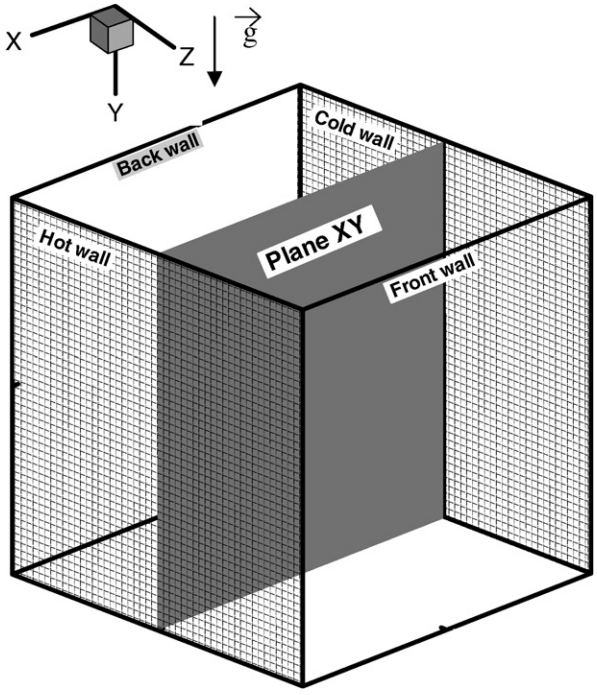

Fig. 1. The physical model and the coordinate system.

cavity instead of being confined to the front and back walls. In 3D rectangular enclosure, Henry and Buffat (1998) founded that particles spiral from the lateral walls towards the XY-mid-plane with an increasing radius, return to the lateral walls by a large spiral plane along the walls and then flow inwardly the lateral walls. For this category of fluids, both Juel et al. (2001) and Henry and Buffat (1998) declared the three-dimensional cross-flows responsible of the oscillatory convection. This is different then Janssen et al. (1993) results for an air filled cavity for which the instability mechanism responsible for the bifurcation is the same in 2D and 3D cases. More detailed bibliography on this subject can be found in the work of Piazza and Ciofalo (2002).

Several two-dimensional studies are found for the problem of combined radiation and natural convection in rectangular participating medium (Chang et al., 1983; Yang, 1986; Yucel et al., 1989; Fusegi and Farouk, 1989; Tan and Howell, 1991). A recent 3D numerical simulation of radiation and convection in a differentially heated cubic cavity using the discrete ordinates method is effectuated by Colomer et al. (2004). The authors detail the effect of the Planck number and the optical thickness on heat transfer and effectuate a comparison between dimensional results obtained from a two-dimensional model and those obtained in the mid-plane of a long rectangular enclosure. But, no special focus is given to the effect of radiation on the three-dimensional spiraling flow.

In the present work, the qualitative effect of the radiative heat transfer on the three-dimensional convection of a cubic radiatively participating melt with $Pr = 13.6$ and $Ra = 10^5$ is investigated for different optical parameters of the medium. The structure of the main flow is considerably altered when changing the value of the conduction–radiation parameter. The inner spiraling flows are found very sensible in location and direction to the radiative heat transfer. However, the peripheral spiraling motion is qualitatively insensitive to these parameters. In the following and after the formulation of the problem and some validations of the numerical code, the first results concern the main flow and heat transfer and the second the transverse spiraling flow.

2. Formulation

As shown in Fig. 1, the physical system consists of a cubic box with uniform imposed temperatures at two opposite vertical walls and adiabatic top, bottom, front and back walls. All these walls are assumed to be gray and diffuse. The medium is considered as a gray, emitting–absorbing and isotropically scattering fluid. Initially, the medium and the box are at a uniform temperature T'_c, while the temperature of the left vertical wall are suddenly changed to higher value T'_h and the temperature on the right wall is maintained at T'_c. It is assumed that the flow in the system is laminar with no-slip conditions at the walls, the physical properties are constant, and the Boussinesq approximation is valid. The viscous dissipation and the work of pressure forces are negligible.

Scaling length, velocity, and time are dimensionless by W, α/W and W^2/α, and defining dimensionless temperature as $T = (T' - T'_c)/(T'_h - T'_c)$, the governing equations in dimensionless vorticity vector potential form are:

$$\vec{\nabla}^2\vec{\phi} = -\vec{\omega} \tag{1}$$

$$\frac{\partial\vec{\omega}}{\partial t} + (\vec{V}.\vec{\nabla})\vec{\omega} - (\vec{\omega}.\vec{\nabla})\vec{V} = \vec{\nabla}^2\vec{\omega} + PrRa\left[\frac{\partial T}{\partial z}, 0, -\frac{\partial T}{\partial x}\right] \tag{2}$$

$$\frac{\partial T}{\partial t} + (\vec{V}.\vec{\nabla})T = \vec{\nabla}^2 T + \frac{\mathrm{Rc}\tau}{\Phi\pi}(1-\omega_0)\left[\int I\,\mathrm{d}\Omega - 4\pi(1+\Phi T)^4\right] \tag{3}$$

where,

$$\vec{\omega} = \vec{\nabla}\times\vec{V} \tag{4}$$

$$\vec{V} = \vec{\nabla}\times\vec{\phi} \tag{5}$$

$$\vec{\nabla} = \frac{\partial}{\partial x}\vec{i} + \frac{\partial}{\partial y}\vec{j} + \frac{\partial}{\partial z}\vec{k} \tag{6}$$

The Foregoing dimensionless parameters are given as follows: Prandtl number $Pr = \frac{\nu}{\alpha}$, Rayleigh number $Ra = \frac{g\beta_T(T'_h - T'_c)W^3}{\alpha\nu}$, temperature ratio $\Phi = \frac{T'_h}{T'_c} - 1$ and the conduction–radiation interaction parameter $\mathrm{Rc} = n^2\frac{W\sigma T'^3_c}{\lambda}$. The boundary conditions for the considered problem are (Wakashima and Saitoh, 2004): Hot wall ($x = 1$)

$$T = 1, \quad \omega_1 = 0, \quad \phi_2 = \phi_3 = \frac{\partial \phi_1}{\partial x} = 0,$$
$$\omega_2 = -\frac{\partial V_3}{\partial x}, \quad \omega_3 = \frac{\partial V_2}{\partial x} \tag{7}$$

Cold wall ($x = 0$)

$$T = 0, \quad \omega_1 = 0, \quad \phi_2 = \phi_3 = \frac{\partial \phi_1}{\partial x} = 0,$$
$$\omega_2 = -\frac{\partial V_3}{\partial x}, \quad \omega_3 = \frac{\partial V_2}{\partial x} \tag{8}$$

Bottom and top walls ($y = 0$, 1)

$$-\frac{\partial T}{\partial y} + q_r \mathrm{Rc}/\Phi = 0, \quad \omega_2 = 0, \quad \phi_1 = \phi_3 = \frac{\partial \phi_2}{\partial y} = 0,$$
$$\omega_1 = \frac{\partial V_3}{\partial y}, \quad \omega_3 = -\frac{\partial V_1}{\partial y} \tag{9}$$

Front and back walls ($z = 0$, 1)

$$-\frac{\partial T}{\partial z} + q_r \mathrm{Rc}/\Phi = 0, \quad \omega_3 = 0, \quad \phi_1 = \phi_2 = \frac{\partial \phi_3}{\partial z} = 0,$$
$$\omega_1 = -\frac{\partial V_2}{\partial z}, \quad \omega_2 = \frac{\partial V_1}{\partial z} \tag{10}$$

and $V_1 = V_2 = V_3 = 0$ on all walls.

The radiative transfer equation, in absorbing–emitting and isotropically scattering medium, can be written as (Siegel and Howell, 1992; Borjini et al., 2003).

$$\frac{\partial I(s, \mathbf{\Omega})}{\partial s} + \beta_r I(s, \mathbf{\Omega}) = \beta_r R \tag{11}$$

where

$$R = (1 - \omega_0) I^0(s) + \frac{\omega_0}{4\pi} \int_{4\pi} I(s, \mathbf{\Omega}) \mathrm{d}\Omega \tag{12}$$

The FTn finite volume method is utilized to discretize Eq. (11). The computational domain is divided into finite volumes and the intensity direction into finite number of solid angles. The angular discretization of this method is recommended for 3D problems because it reduces the ray effect and the error due to non-symmetric angular discretization under rotation of the three axes (Kim and Huh, 2000; Guedri et al., 2006). This equation is integrated over each control volume and control angle. Using the step scheme, one get the following system of algebraic coupled equations in three-dimensional formulation (Guedri et al., 2006).

$$a_p^l I_p^l = a_W^l I_W^l + a_E^l I_E^l + a_S^l I_S^l + a_N^l I_N^l + a_B^l I_B^l + a_T^l I_T^l + b_P \tag{13}$$

where

$$a_W^l = \Delta A_w \max[-N_w^l, 0] \tag{14}$$
$$a_E^l = \Delta A_e \max[-N_e^l, 0] \tag{15}$$
$$a_N^l = \Delta A_n \max[-N_n^l, 0] \tag{16}$$
$$a_S^l = \Delta A_s \max[-N_s^l, 0] \tag{17}$$
$$a_B^l = \Delta A_b \max[-N_b^l, 0] \tag{18}$$
$$a_T^l = \Delta A_t \max[-N_t^l, 0] \tag{19}$$
$$a_p^l = \Delta A_w \max[N_w^l, 0] + \Delta A_e \max[N_e^l, 0] + \Delta A_s \max[N_s^l, 0] + \Delta A_n \max[N_n^l, 0] + \Delta A_b \max[N_b^l, 0] + \Delta A_t \max[N_t^l, 0] + \beta \Delta v_p \tag{20}$$
$$b_P = \beta_r R_p \Delta v_p \tag{21}$$

For gray and diffuse surface, the dimensionless radiative boundary conditions are:

$$I_W^l = \varepsilon (1 + \Phi T)^4 + (1 - \varepsilon) \sum_{L_+} \left| N_W^{l'} \right| I_W^{l'} \Delta \Omega^{l'} \tag{22}$$

More details on the finite volume method are in Chai et al. (1994) and Guedri et al. (2006).The dimensionless conductive and radiative fluxes are evaluated along the isothermal walls as follows:

Local conductive flux

$$q_c = -\frac{\partial T}{\partial x} \tag{23}$$

Local radiative flux

$$q_r = \sum_{l=1}^{L} N^l I^l \Delta \Omega^l \tag{24}$$

The averaged values on isothermal walls of these quantities are denoted $\bar{q}_c$ and $\bar{q}_r$ respectively.

Eqs. (1)–(3) are discretized using the control volume finite difference method (Patankar, 1980). The central-difference scheme for treating convective terms and the fully implicit procedure to discretize the temporal derivatives are retained. The grid is uniform in all directions with additional nodes on boundaries. The resulting non-linear algebraic equations are solved using the successive relaxation-iterating scheme (Bejan, 1984). The equation of radiative transfer is solved by repeatedly sweeping across grid until convergence without taking into account the optimal order in which the nodes should be visited. More details on the present numerical algorithm are in the works of Borjini et al. (2003) and Guedri et al. (2006). The time step 10^{-4}, spatial mesh 51^3 and the angular mesh of the FT_6FVM are retained to carry out all numerical tests. The solution is considered acceptable when the following convergence criterion is satisfied for each step of time and for each dependent variable Δ.

$$\frac{\max |\Delta^m - \Delta^{m-1}|}{\max |\Delta^m|} \leqslant 10^{-5} \tag{25}$$

where the superscript m designates the iteration number.

3. Validation tests

Results in the absence of radiation are compared, in Table 1, with the benchmark solutions of Wakashima and Saitoh (2004) with air and for different Rayleigh

Table 1
Comparison between the present results and literature for non-radiative fluid, $Pr = 0.71$

		$\phi_3/\sqrt{Pr \cdot Ra}$ (center)	$\omega_3/\sqrt{Pr \cdot Ra}$ (center)	S (center)	$\bar{q}_c$
$Ra = 10^4$	Present results	0.05573	1.1091	0.8617	2.06242
	Wakashima and Saitoh (2004)	0.05492	1.1018	0.8634	2.0624
	Deviation (%)	1.47	0.66	0.19	0.01
$Ra = 10^5$	Present results	0.03452	0.2583	1.0836	4.3771
	Wakashima and Saitoh (2004)	0.03403	0.2573	1.0867	4.3668
	Deviation (%)	1.44	0.39	0.29	0.24

Table 2
Comparison of heat transfer on the hot wall between the present results and Colomer et al. results (2004) (quantities in the parentheses) for radiative fluid, $Pr = 0.71$, $Rc = 1/(0.016 \times 17)$, and $\Phi = 1/17$

		$\tau = 0$	1	10
$Ra = 10^3$	$\bar{q}_c$	1.057 (*1.76*)	1.698 (*1.76*)	1.651 (***1.54***)
	$\bar{q}_r Rc/\Phi$	6.487 (*6.20*)	4.612 (*4.64*)	1.2469 (***1.16***)
10^4	$\bar{q}_c$	2.038 (*2.26*)	2.45 (*2.25*)	2.229 (***2.11***)
	$\bar{q}_r Rc/\Phi$	6.89 (*6.28*)	5.122 (*4.69*)	1.65 (***1.54***)
10^5	$\bar{q}_c$	4.133 (***4.37***)	4.038 (***3.92***)	4.458 (***4.21***)
	$\bar{q}_r Rc/\Phi$	7.227 (***6.52***)	5.88 (***5.44***)	2.992 (***2.8***)

numbers. The deviations for both the flow and heat transfer variables are tolerable for three-dimensional modeling (Pepper and Hollands, 2002). The validation of the three-dimensional radiative component of the present code can be found in Borjini et al. (2003)and Guedri et al. (2006). For the combined model, comparison of radiative and conductive heat fluxes on the hot wall, with the recent results of Colomer et al. (2004), is presented, in Table 2, for different optical thicknesses. A remarkable difference is observed between the two results for both radiative and conductive components of the heat flux. It is important to signal that Colomer et al. (2004) used the Discrete Ordinates Method with appropriate directions and for the 3D idealized classical furnace they compare the radiative heat flux only with the P3 method results.

4. Results and discussion

The effect of the radiative heat transfer on the characteristics of the main flow and the three-dimensional cross flow will be discussed for $Ra = 10^5$, $Pr = 13.6$, $\Phi = 0.1$, black isothermal walls and perfectly reflecting adiabatic walls. This Prandtl number corresponds to the radiatively participating $LiNbO_3$ melt (Kobayachi et al., 2000). Firstly, the effects of the conduction-to radiation parameter, optical thickness and scattering albedo on the main flow and heat transfer are rapidly discussed. Secondly, the three-dimensional behavior of the flow is analyzed for absorbing–emitting medium and for different optical widths. In the following, for simplicity and due to the symmetry of the problem, only the half of the enclosure is interpreted.

4.1. Effect of radiation on the main flow

In the absence of any contrary indication, an absorbing–emitting medium with $\tau = 1$ is used. In Fig. 2, is represented the velocity projection on the XY plane for $Rc = 0$ (without radiation), 10 and ∞ (radiation-induced natural convection). The same vector-size scale is used for all cases. In absence of the radiative transfer, a 'cats eye' flow slightly titled toward the cold wall is established. When Rc increases the flow in the core is intensified and only one vortex is observed. This grouping of the two separate cores is already predicted in 2D simulation (Tan and Howell, 1991). However, with the 3D modeling, the streamlines in the xy-planes are not closed. For instance, in the core and for $Rc \to \infty$ a convergent quasi-logarithmic spiral motion is established for $z = 0.5$. Near the back and front walls, a divergent more pronounced quasi-logarithmic spiral motion takes place (this behavior will be discussed later). The corresponding isothermal surfaces shown in Fig. 3 bring to the fore the decrease of the vertical thermal stratification in the center when the medium is radiatively participating. This dressing up of isotherms is due to the radiative heating of the fluid near the top of the hot wall and near the bottom of the cold wall. One notes the 3D distribution of temperature for $Rc = 0$ and 10. For $Rc \to \infty$, the temperature field is independent of the flow field and the pure radiative profile of isotherms is obtained. These isothermal surfaces are quasi-equidistant except near the active walls. The distributions of conductive and radiative heat fluxes on the hot wall for $Rc = 0$, 1 and ∞ are represented in Fig. 4. It is remarkable that radiation increases conductive heat transfer at the top of the hot wall and decreases it at the bottom and the reverse is true for the cold wall (results not represented here but easily deduced by inversing the y-direction in Fig. 4). Due to the temperature levels, the radiative flux is higher on the hot wall while the conductive flux is more important on the cold wall. For $Rc = 0$, there are maximums of heat transfer at the top of the cold wall and at the bottom of the hot wall. The radiative heat transfer tends to homogenize these distributions. These characteristics are qualitatively similar to those obtained for air with 3D (Colomer et al., 2004) or 2D (Tan and Howell, 1991) computations. As predicted for $Rc \to \infty$, the heat flux distributions do not present any effect of gravity and are almost identical on hot and cold walls. Colomer et al. (2004) also observed an increase of the heat flux at both ends of z axis. This increase is more important for optical thin media. Fig. 4 shows also that the side walls effects on conductive heat transfer are more pronounced at the bottom of the hot wall and the top of

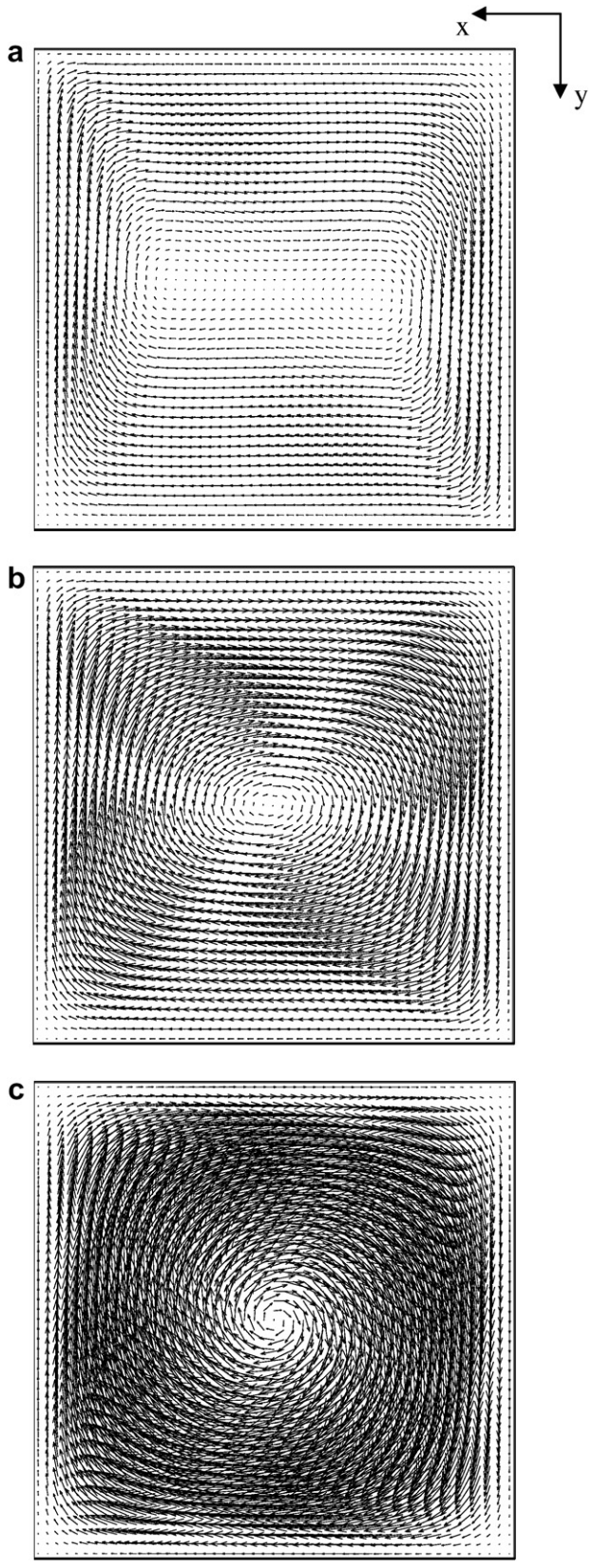

Fig. 2. Influence of the radiation–conduction parameter on the velocity vectors projected onto the XY-mid-plane for $Ra = 10^5$, $Pr = 13.6$ and $\tau = 1$. (a) $\mathrm{Rc} = 0$; (b) $\mathrm{Rc} = 10$; and (c) $\mathrm{Rc} = \infty$.

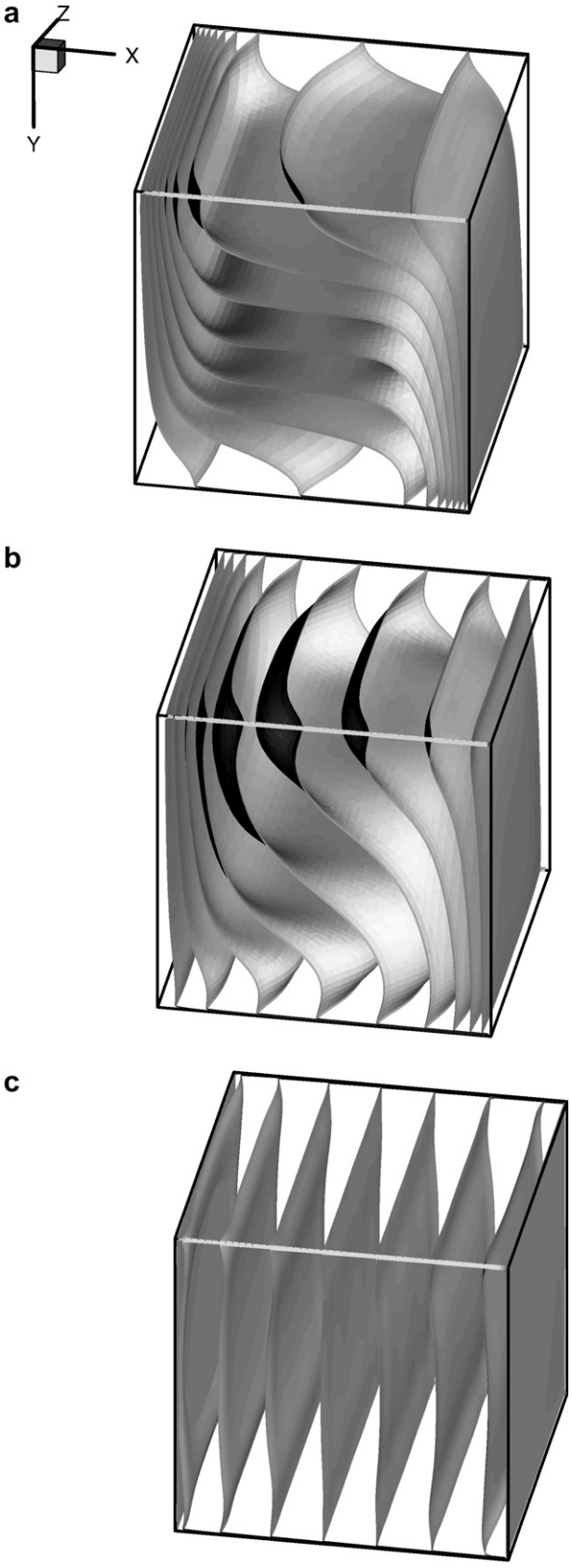

Fig. 3. Effect of the radiation–conduction parameter on temperature distribution for $Ra = 10^5$, $Pr = 13.6$ and $\tau = 1$. (a) $\mathrm{Rc} = 0$; (b) $\mathrm{Rc} = 10$; and (c) $\mathrm{Rc} = \infty$.

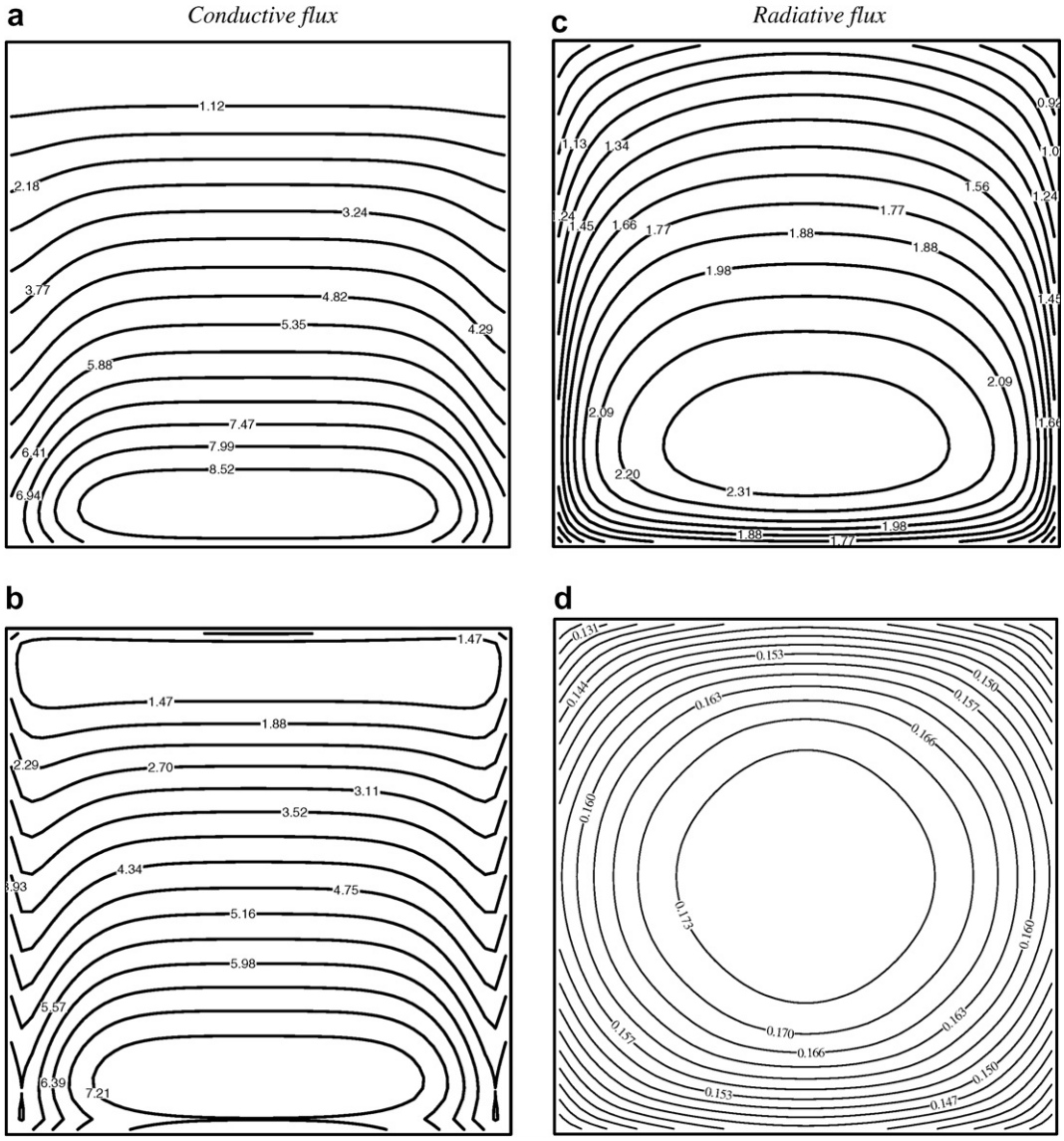

Fig. 4. Effect of the radiation–conduction parameter on local conductive and radiative flux distributions on hot wall for $Ra = 10^5$, $Pr = 13.6$ and $\tau = 1$. (a) iso-values of $\bar{q}_c$ for $Rc = 0$; (b) iso-values of $\bar{q}_c$ for $Rc = 1$; (c) iso-values of $\bar{q}_r.Rc/\Phi$ for $Rc = 1$; (d) iso-values of $\bar{q}_r$ for $Rc = \infty$.

the cold wall. The reverse is true for the radiative heat flux. Table 3 resumes the effect of radiative properties on averaged heat transfer on the active walls for $Rc = 1$. Like in the results for an air filled square cavity (Tan and Howell, 1991), the optical width has more significant effect than the scattering albedo. The strong dependency of $\bar{q}_r$ on τ is obvious according to this table.

Table 3
Effect of optical parameters on heat transfer for $Ra = 10^5$, $Pr = 13.6$, and $Rc = 1$

		Hot wall		Cold wall	
τ	ω_0	$\bar{q}_c$	$\bar{q}_r Rc/\Phi$	$\bar{q}_c$	$\bar{q}_r Rc/\Phi$
0.1	0	4.503	2.115	4.541	2.055
1	0	4.335	1.845	4.465	1.688
10	0	4.538	1.017	4.664	0.8774
1	0.5	4.387	1.77	4.484	1.649
1	0.9	4.488	1.655	4.542	1.615

4.2. Effect of radiation on the transverse flow

The transverse flow is a direct manifestation of the 3D nature of the flow and it is primordial to study time-dependency and transition. This three-dimensional motion is generated by the presence of no-slip end walls (Mallinson and de Vahl Davis, 1977) which provokes the 3D inertial-end effect and by the 3D thermal-end effect (temperature gradient near the side-walls). For Rayleigh–Benard air convection, Kessler (1987) mentioned that thermal effects are restricted to a small zone near the walls while the inertial effects are perceptible in the whole box. In fact, and as mentioned above, the parcel of particles that are traveling in the xy planes did not stay on the same plane

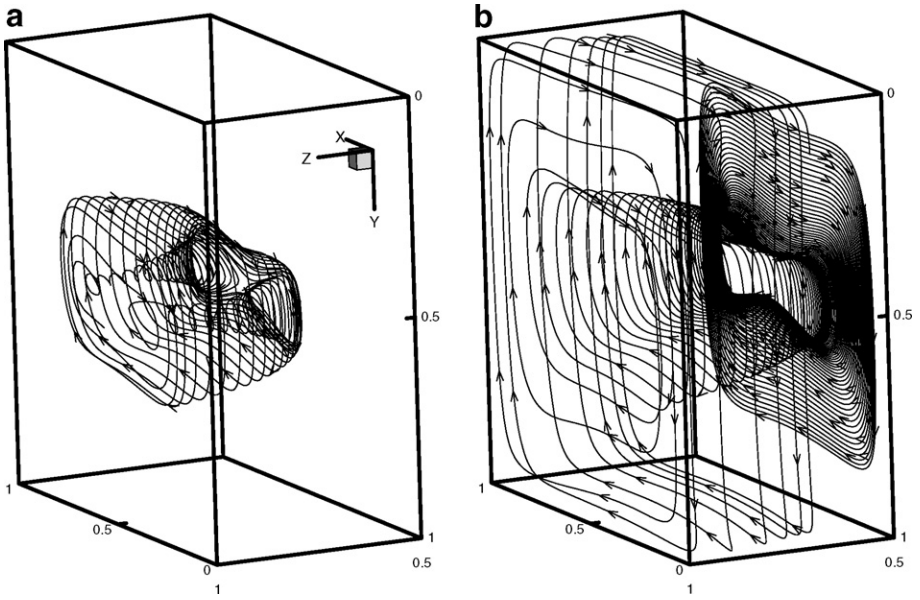

Fig. 5. Some particle tracks in absence of radiation, for $Ra = 10^5$ and $Pr = 13.6$ showing inner spiraling flows (a) and 'peripheral' spiraling flows (b).

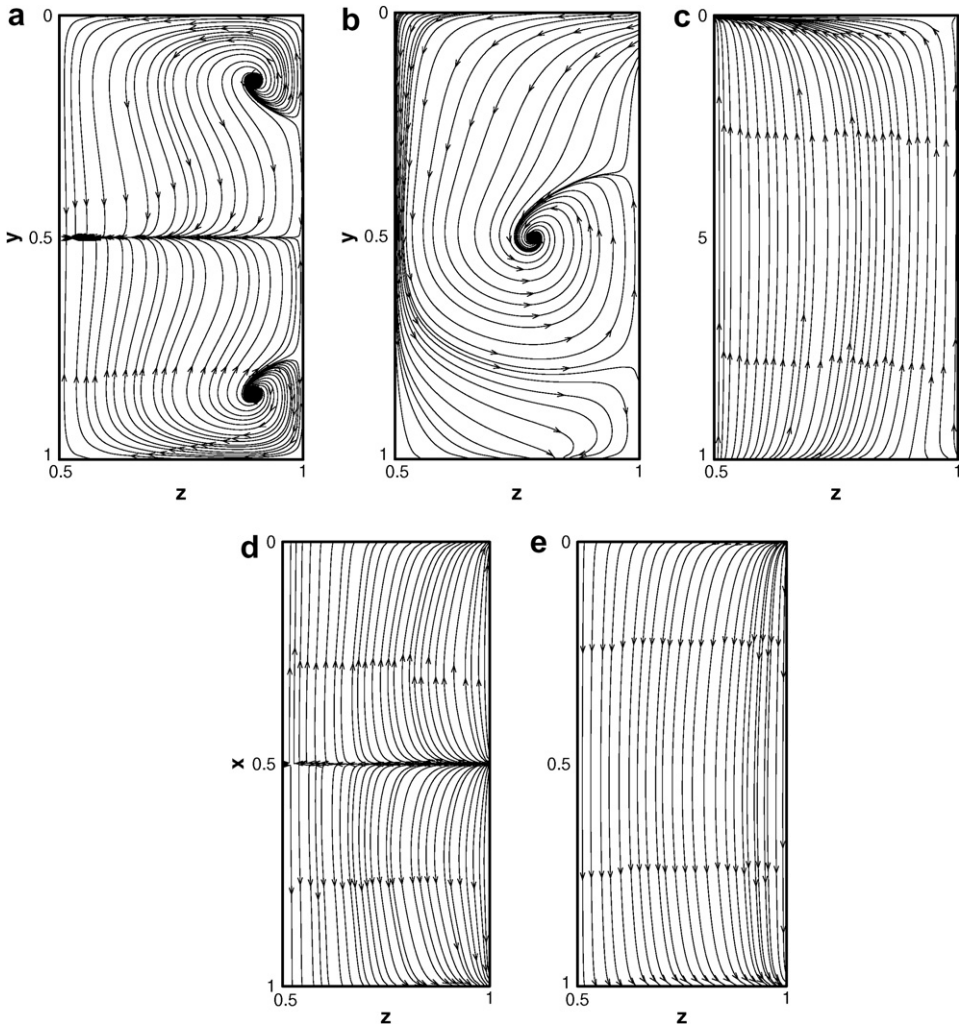

Fig. 6. Projections of flow lines on the yz and xz planes in absence of radiation, for $Ra = 10^5$ and $Pr = 13.6$. (a) $x = 0.5$; (b) $x = 0.68$; (c) $x = 0.9$; (d) $y = 0.5$; (e) $y = 0.9$.

and a weak 'helically' flow exists. The corresponding velocity component V_3 is in general an order of magnitude smaller than the main flow (V_1 and V_2) (Fusegi et al., 1991a; Wakashima and Saitoh, 2004). Contrary to the two-dimensional flow, the projection of streamlines in the XY plane are not closed but spirals towards the center of the vortices or toward the side walls.

It will be shown in the following results that different globally convergent or divergent spiraling flows towards the central XY plane take place and the effect of the radiative heat transfer on three-dimensional convection is clearly identified in the core of the box. In fact, in the presence of radiation, a divergent inner spiraling flow is established while for $\mathrm{Rc} = 0$, this central transverse flow is convergent. However, the flow at the periphery is always globally convergent towards the XY plane independently of the radiative behavior of the fluid.

Before beginning the depictions of these spiraling flows, special tests with three different Prandtl numbers are effectuated. The results giving some particles tracks for $Pr = 6300$ and $Ra = 7.910^4$ (figure not shown here), concords globally with the experimental and the numerical results of Hiller et al. (1989) and Kowalewski (1998). In fact, near the centers of the front and the back walls, the streamlines split into two spiraling convergent flows toward the XY-mid-plane. After this, the streamlines circulate back toward these walls and finally, toward the XY plane near the side walls. The results are sensibly the same for $Pr = 0.71$ and $Ra = 10^5$ but the inner spiraling flow is directed toward the front and back walls. For lower Prandtl numbers ($Pr = 0.05$) and for $Ra = 10^5$, the solution is oscillatory with two-vortices-main-structure flow. Furthermore, the inner spiraling motion is more complicated and the 3D effects are intensified near the center of the XY-mid-plane of the cavity. This is globally in line with the conclusions of Viskanta et al. (1986).

For $Pr = 13.6$, $Ra = 10^5$, and for the case without radiation, a different and more complex transverse flow is registered. In fact, two central spiraling motions exist and converge toward the intermediate xy-plane situated at $z \approx 0.65$ (Fig. 5a). This is followed by a divergent flow until the front wall as shown in this figure. After this, a succession of convergent, divergent and convergent spiraling flows between this wall and the plane XY is accomplished (Fig. 5b). Fig. 6a–c represent the projection of the streamlines on the yz plane for three distinct x positions. Near the periphery ($x = 0.9$) and despite that the flow is globally convergent toward the central plane XY, a local divergent flow is registered which invokes a 'concavity', in the yz plane of the streamlines. The cross-flow structure is more complex for $x = 0.5$ and in the zone situated between the two inner spirals and the XY plane ($0.5 < z < 0.65$), the three-dimensional velocity V_3 is relatively very weak which can define a quasi-2D region. The two appearing vortices in this figure are monitoring the aforementioned succession of convergent and divergent flows. Furthermore, in the plane $x = 0.68$ which splits one inner spiral, the vertical superposition of convergent and divergent flows is obvious. The corresponding results for the plane xz are represented in Fig. 6d and e. For $y = 0.9$, the projection of the streamlines brings to the fore the 'convexity' towards the plane XY, of

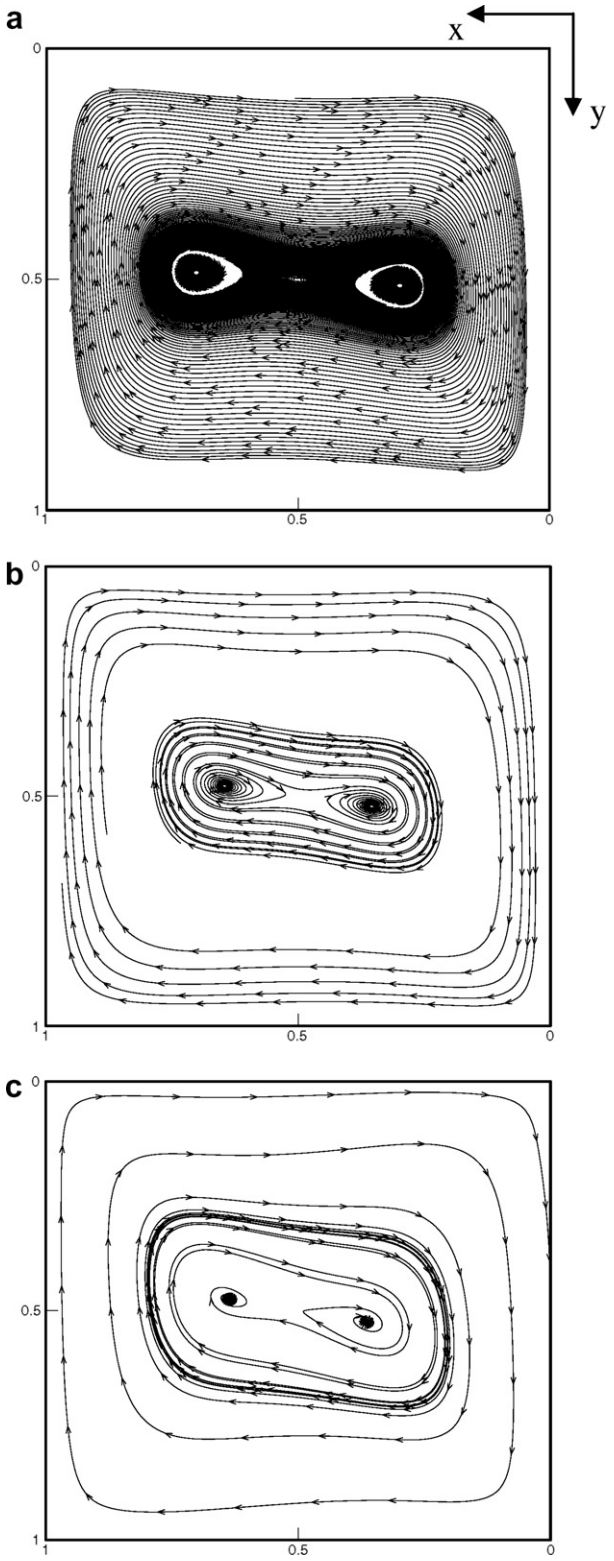

Fig. 7. Projections of streamlines in the xy plane, without radiation, for $\mathrm{Ra} = 10^5$ and $\mathrm{Pr} = 13.6$. (a) $z = 0.5$; (b) $z = 0.9$; and (c) $z = 0.99$.

the converging peripheral spiral flow. The quasi-2D zone is clearly discernible in the plane $y = 0.5$ and near $z = 0.5$ (except on the axe $x = 0.5$). As mentioned above, the streamlines in the xy planes are not closed. This is confirmed in Fig. 7a which shows convergent motion toward the two vortices in the XY plane. This structure is modified for $z = 0.9$ and the projections of peripheral streamlines spiral towards the walls (Fig. 7b). This structure persists until $z = 0.99$ (Fig. 7c) and consequently no merging of the vortices is observed. While in the center the flow stills convergent toward the centers of these vortices.

The above results are dramatically altered by the surface to surface and the internal radiative heat transfers. For $\mathrm{Rc} = 1$ and $\tau = 0.1$, the inner spiraling flow is divergent and works directly between the XY plane and the front and back walls (Fig. 8a). The merging of the two vortices occurs between this plane and the cited walls. The particle track displayed in Fig. 8b resumes both inner divergent and peripheral convergent transverse spiraling flows. The peripheral convergent flow is similar to which obtained in pure natural convection. In addition, the abovementioned 'concavity' and 'convexity' in the plane $x = 0.9$ and $y = 0.9$, respectively, are retrieved (figure not shown here). However, for $y = 0.5$ (Fig. 9b), a great change is observed and the flow is clearly divergent from the plane XY. The projections of streamlines in the $x = 0.5$ plane (Fig. 9a) are also considerably different from those obtained without radiation and the symmetry between the flows into the top and bottom quadrants is broken. These results demonstrate that radiative heat transfer increases the three-dimensional transverse flow in the center of the enclosure and so restricts the aforementioned quasi-2D zone. In fact, for $z = 0.8$, the initial central two-vortices-flow (Fig. 10a) changes and the streamlines become divergent (spiral

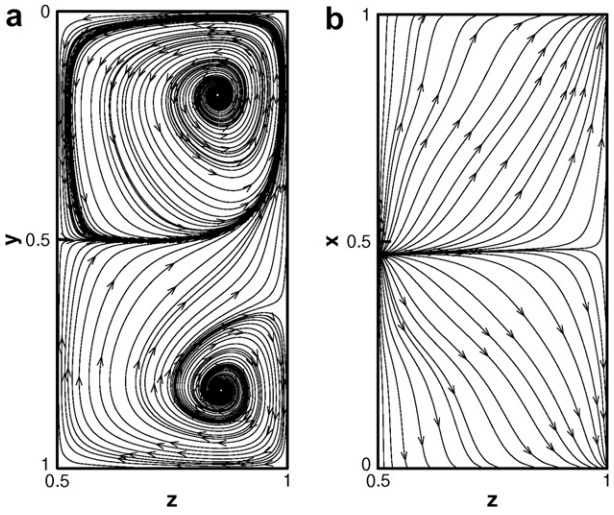

Fig. 9. Projections of flow lines on the yz and xz planes, for $Ra = 10^5$, $Pr = 13.6$, $\mathrm{Rc} = 1$ and $\tau = 0.1$. (a) $x = 0.5$; (b) $y = 0.5$.

toward the boundaries) while the outer streamlines still convergent (Fig. 10b). For $z = 0.85$ the two vortices merge into one vortex (Fig. 10c) and at $z = 0.9$ all the flow is divergent. So, for radiatively participating fluid, the main flow manifests an one-vortex structure near the front and back walls even with moderate value of the conduction–radiation parameter ($\mathrm{Rc} = 1$).

The results for $\tau = 1$ and 10 are qualitatively analogous to those for $\tau = 0.1$. However, when the optical thickness increases, the radius of the central-helically diverging motions increases and the merging of the two vortices occurs near the plane XY. In other tests, the values of $\omega_0 = 0.5$, 0.9 do not influence the structure of the transverse flow.

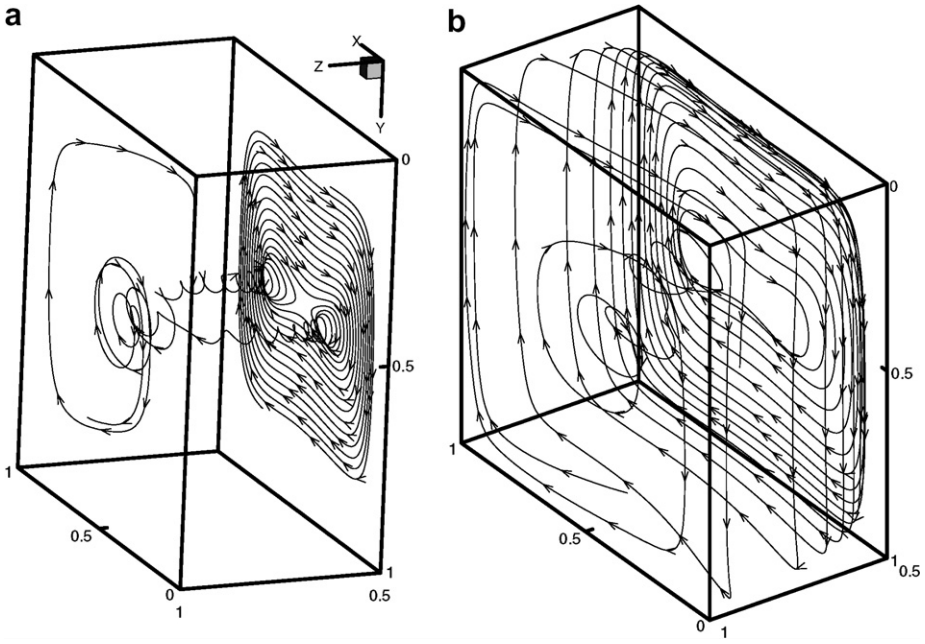

Fig. 8. Some particle tracks for $Ra = 10^5$, $Pr = 13.6$, $\mathrm{Rc} = 1$, $\tau = 0.1$ showing inner spiraling flows (a) and 'peripheral' spiraling flows (b).

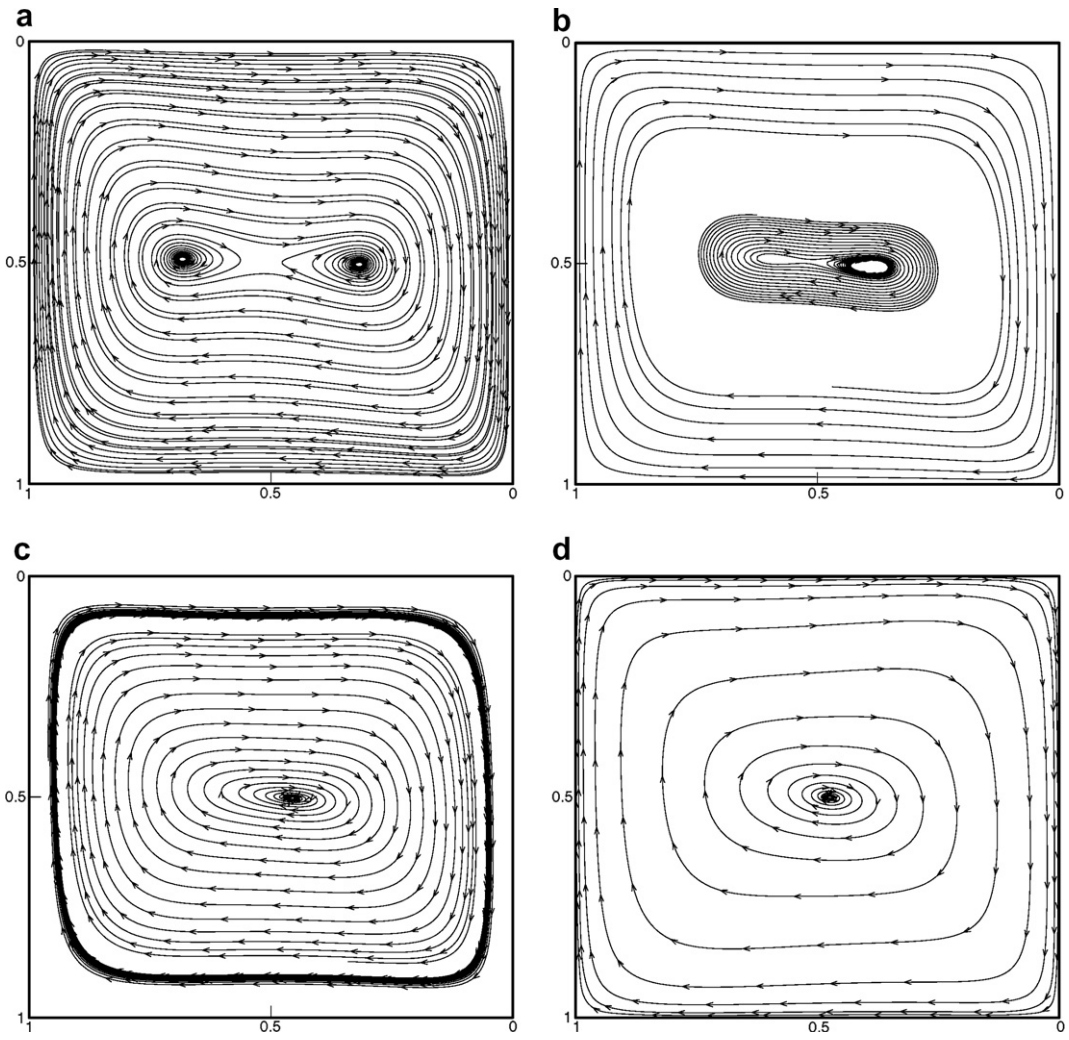

Fig. 10. Projections of streamlines in the xy plane, for $Ra = 10^5$, $Pr = 13.6$, Rc = 1 and $\tau = 0.1$. (a) $z = 0.5$; (b) $z = 0.8$; (c) $z = 0.85$; and (d) $z = 0.9$.

5. Conclusion

The present numerical results show, for $Pr = 13.6$ and in absence of radiation, the existence of a quasi-2D zone far from the end walls and near the center of the XY-mid-plane. The inner spiraling transverse flow begins half away between this plane and the front and back walls.

The effect of the radiative heat transfer on the 3D behavior of the flow is significant in the core of the enclosure. The inner spiraling flows are found very sensible in location and direction to the radiative heat transfer, while the peripheral spiraling motion is qualitatively insensitive to this mode. This postulates that radiative heat transfer conveys the 3D-thermal-end-effect to the bulk of the cavity. In fact, the inner convergent spiraling flow occurring in pure natural convection becomes oriented toward the front and back walls in presence of internal radiation. However, the flow at the periphery is convergent toward the XY-mid-plane for both radiatively participating and non-participating fluid.

In the absence of radiation and near the front and back walls, the fluid at the periphery spirals outwardly and no combination of the two vortices is observed. However, for a semitransparent medium and when approaching the front and back walls, the particles in the center flow outwardly and a combination of the two vortices is observed. The location of this merging and the radius of the helically motion are sensible to the optical thickness while the scattering albedo is without effect on the spiraling transverse flow.

This is true for a moderately radiatively participating fluid. In fact, when radiation is predominant (important value of Rc), even the structure of the flow in the XY-mid-plane is altered by this mode of heat transfer.

The results of the present topological analysis justifies a future quantitative parametric study of the effect of radiation on the 3D characteristics of the flow in a differentially heated cubic enclosure.

References

Bejan, A., 1984. Convection Heat Transfer. John Wiley and Sons, New York.

Borjini, M.N., Farhat, H., Radhouani, M.S., 2003. Analysis of radiative heat transfer in a partitioned idealized furnace. Numerical Heat Transfer, Part A 44, 199–218.

Chai, J.C., Lee, H.S., Patankar, S.V., 1994. Finite volume method for radiative heat transfer. Journal of Thermophysics and Heat Transfer 8, 419–425.

Chang, L.C., Yang, K.T., Lioyd, J.R., 1983. Radiation-natural convection interactions in two-dimensional complex enclosures. Journal of Heat Transfer 105, 89–95.

Colomer, G., Costa, M., Cònsul, R., Oliva, A., 2004. Three-dimensional numerical simulation of convection and radiation in a differentially heated cavity using the discrete ordinates method. International Journal of Heat Mass Transfer 47, 257–269.

Fusegi, T., Farouk, B., 1989. Laminar and turbulent natural convection–radiation interactions in a square enclosure filled with a nongray gas. Numerical Heat Transfer 15, 303–322.

Fusegi, T., Hyun, J.M., Kuwahara, K., Farouk, B., 1991a. A numerical study of three-dimensional natural convection in a differentially heated cubical enclosure. International Journal of Heat Mass Transfer 34, 1543–1557.

Fusegi, T., Hyun, J.M., Kuwahara, K., 1991b. A numerical study of 3-D natural convection in a cube: effects of the horizontal thermal boundary conditions. Fluid Dynamics Research 8, 221–230.

Fusegi, T., Hyun, J.M., Kuwahara, K., 1992. Numerical simulations of natural convection in a differentially heated cubical enclosure with a partition. International Journal of Heat Fluid Flow 13, 176–183.

Fusegi, T., Hyun, J.M., 1994. Laminar and transitional natural convection in an enclosure with complex and realistic conditions. International Journal of Heat Fluid Flow 15, 258–268.

Guedri, K., Borjini, M.N., Mechi, R., Said, R., 2006. Formulation and testing of the FTn finite volume method for radiation in 3-D complex inhomogeneous participating media. Journal of Quantitative Spectroscopy and Radiative Transfer 98, 425–445.

Henry, D., Buffat, M., 1998. Two and three-dimensional numerical simulations of the transition to oscillatory convection in low-Prandtl fluids. Journal of Fluid Mechanics 374, 145–171.

Hiller, W.J., Koch, S., Kowaleweski, T.A., 1989. Three-dimensional structures in laminar natural convection in a cubic enclosure. Experimental Thermal and Fluid Science 2, 34–44.

Hiller, W.J., Koch, S., Kowaleweski, T.A., de Vahl Davis, G., Behnia, M., 1990. Experimental and numerical investigation of natural convection in a cube with two heated side walls. Proceedings of the International Union of Theoretical and Applied Mechanics Symposium, 717–726.

Janssen, R.J.A., Henkes, R.A.W.M., Hoogendoorn, C.J., 1993. Transition to time-periodicity of a natural-convection flow in a 3D differentially heated cavity. International Journal of Heat Mass Transfer 36, 2927–2940.

Juel, A., Mulin, T., Ben Hadid, H., Henry, D., 2001. Three-dimensional free convection in molten gallium. Journal of Fluid Mechanics 436, 267–281.

Kessler, R., 1987. Nonlinear transition in three-dimensional convection. Journal of Fluid Mechanics 174, 357–379.

Kim, S.H., Huh, K.Y., 2000. A new angular discretization scheme of the finite volume method for 3-D radiative heat transfer in absorbing, emitting and anisotropically scattering media. International Journal of Heat Mass Transfer 43, 1233–1242.

Kobayachi, M., Tsukada, T., Hozawa, M., 2000. Effect of internal radiative heat transfer on transition of flow modes in CZ oxide melt. Journal of Crystal Growth 208, 459–465.

Kowalewski, T.A., 1998. Experimental validation of numerical codes in thermally driven flows, in Advance Computational Heat Transfer. Begel House Inc., Ny, pp. 1–15.

Lee, T.S., Son, G.H., Lee, J.S., 1988. predictions of three-dimensional natural convection in a box. Proceedings of the 1st KSME–JSME Thermal and Fluid Engineering Conference 2, 278–283.

Leonardi, E., Kowalewski, T.A., Timchenko, V., de Vahl Davis, G., 1999. Effects of finite wall conductivity on flow structures in natural convection. In: Mohamed, A.A., Sezai, I. (Eds.), CHMT Cyprus April 1999. Eastern Mediterranean University Printing House, pp. 82–188.

Le Peutrec, Y., Lauriat, G., 1990. Effects of the heat transfer at the side walls on natural convection in cavities. Journal of Heat Transfer 112, 370–378.

Mallinson, G.D., de Vahl Davis, G., 1977. Three-dimensional natural convection in a box: a numerical study. Journal of Fluid Mechanics 83, 1–31.

Patankar, S.V., 1980. Numerical Heat Transfer and Fluid Flow. McGraw Hill, New York.

Pepper, D.W., Hollands, K.G.T., 2002. Summary of benchmark numerical studies for 3-D natural convection in an air-filled enclosure. Numerical Heat Transfer, Part A 42, 1–11.

Piazza, I.D., Ciofalo, M., 2002. MHD free convection in a liquid–metal filled cubic enclosure. I. Differential heating. International Journal of Heat Mass Transfer 45, 1477–1492.

Salat, J., Xin, S., Joubert, P., Sergent, A., Penot, F., Le Quéré, P., 2004. Experimental and numerical investigations of turbulent natural convection in a large air-filled cavity. International Journal of Heat Fluid Flow 25, 1034–1046.

Siegel, R., Howell, J.R., 1992. Thermal Radiation Heat Transfer, 3rd ed. Hemisphere Publishing Corp., New York.

Tan, Z., Howell, J.R., 1991. Combined radiation and natural convection and in a two-dimensional participating square medium. International Journal of Heat Mass Transfer 34, 785–793.

Tric, E., Labrosse, G., Betrouni, M., 2000. A first incursion into the 3D structure of natural convection of air in a differentially heated cubic cavity, from accurate numerical solutions. International Journal of Heat Mass Transfer 43, 4043–4056.

Viskanta, R., Kim, D.M., Gau, C., 1986. Three-dimensional natural convection heat transfer of a liquid–metal in a cavity. International Journal of Heat Mass Transfer 29, 475–485.

Wakashima, S., Saitoh, T.S., 2004. Benchmark solutions for natural convection in a cubic cavity using the high-order time–space method. International Journal of Heat Mass Transfer 47, 853–864.

Yang, K.T., 1986. Numerical modelling of natural convection-radiation interactions in enclosures. In: Heat Transfer 1986: Proceedings of the Eighth International Heat Transfer Conference, vol. 1, Hemisphere, Washington, DC, pp. 131–140.

Yucel, A., Acharaya, S., Williams, M.L., 1989. Natural convection and radiation in a square enclosure. Numerical Heat Transfer 15, 261–277.